THE JOURNAL OF PHYSICAL CHEMISTRY Letters

Letter

pubs.acs.org/JPCL

Air-Exposure-Induced Gas-Molecule Incorporation into Spiro-MeOTAD Films

Luis K. Ono,[†] Philip Schulz,[‡] James J. Endres,[‡] Gueorgui O. Nikiforov,[†] Yuichi Kato,[†] Antoine Kahn,[‡] and Yabing Qi*,[†]

[†]Energy Materials and Surface Sciences Unit, Okinawa Institute of Science and Technology Graduate University, 1919-1 Tancha, Onna-son, Kunigami-gun, Okinawa 904-0495, Japan

[‡]Department of Electrical Engineering, Princeton University, Olden Street, Princeton, New Jersey 08544, United States

Supporting Information

ABSTRACT: Combined photoemission and charge-transport property studies of the organic hole transport material 2,2′,7,7′-tetrakis(*N*,*N*-di-*p*-methoxyphenyl-amine)-9,9′-spirobifluorene (spiro-MeOTAD) under air exposure and controlled environments of O_2, H_2O + N_2, and N_2 (1 atm and under dark conditions) reveal the incorporation of gas molecules causing a decrease in charge mobility. Ultraviolet photoelectron spectroscopy shows the Fermi level shifts toward the highest occupied molecular orbital of spiro-MeOTAD when exposed to air, O_2, and H_2O resembling p-type doping. However, no traces of oxidized spiro-MeOTAD$^+$ are observed by X-ray photoelectron spectroscopy (XPS) and UV−visible spectroscopy. The charge-transport properties were investigated by fabricating organic field-effect transistors with the 10 nm active layer at the semiconductor−insulator interface exposed to different gases. The hole mobility decreases substantially upon exposure to air, O_2, and H_2O. In the case of N_2, XPS reveals the incorporation of N_2 molecules into the film, but the decrease in the hole mobility is much smaller.

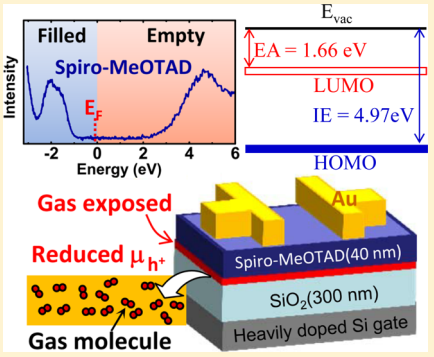

SECTION: Energy Conversion and Storage; Energy and Charge Transport

Solid-state dye-sensitized solar cells (ssDSCs) have received considerable attention due to their potential for high solar power conversion efficiency (PCE) and large-area processing at low cost.[1−4] A typical ssDSC comprises a dye sensitizer in which excitons are induced by light absorption. Subsequent electron injection into the conduction band of mesosporous TiO_2 is accompanied by hole transfer from the oxidized dye to the organic hole transport material (HTM). Further charge transport of electron and hole through the external circuit completes the photovoltaic operation. Various types of sensitizers,[5] including quantum dots[6] and perovskites,[7−14] are currently under investigation. In addition, new HTMs are also under intense investigation as substitutes for the electrolyte triode/iode employed in standard DSCs.[15−17] Today, spiro-MeOTAD is the most widely used HTM in all of the previously mentioned high-performance solid-state cells, mostly due to its amorphous nature (glass-transition temperature T_g = 121 °C) and high solubility.[5,15,18] Material infiltration into the mesosporous TiO_2 layers of up to a few micrometers has been reported.[19] In typical ssDSC devices, additives such as bis(trifluoromethanesulfonyl) (LiTFSI) and 4-*tert*-butylpyridine (*t*-BP) are employed for reducing the charge recombination processes at the spiro-MeOTAD/TiO_2 interfaces.[1,15,20] LiTFSI is also reported to increase the conductivity of spiro-MeOTAD via a doping mechanism, but the fundamental impact of the Li-salt on the energetics of the spiro-MeOTAD/TiO_2 interface remains poorly understood.[21,22] The situation is made even more complex when considering environmental factors (O_2, H_2O, N_2, temperature, and light), which are also known to have a strong influence on the ssDSC device performance. For example, an oxygen-induced doping level increase from 3.5 to 10% in the oxidized spiro-MeOTAD$^+$ species under illumination (photodoping or light soaking step) was reported and proved to be beneficial for producing high PCEs on spiro-MeOTAD-based ssDSC devices.[21−23]

We report on the fundamental interaction between pristine spiro-MeOTAD prepared under ultrahigh vacuum (UHV) conditions and the different gases (O_2, H_2O, and N_2) typically present during the device fabrication steps and storage. The films prepared under UHV conditions make it possible to probe the diffusion of gas molecules and study the changes in the electronic properties of the pristine spiro-MeOTAD films. Such UHV studies combined with controlled gas exposure provide a direct connection with the real fabrication steps, where the device is air-exposed for different periods of time. On the basis of organic field-effect transistor (OFET), ultraviolet photoelectron spectroscopy (UPS), and X-ray photoelectron spectroscopy (XPS) analysis, nitrogen molecules as well as oxygen-containing molecules from the gas phase were observed to

Received: February 25, 2014
Accepted: March 27, 2014
Published: March 27, 2014

diffuse into the film within 25 h. However, only H_2O and O_2 affect the electronic structure of pristine spiro-MeOTAD drastically, while N_2 molecules show weak electronic interaction. Although UPS results point toward a p-type doping effect, we did not observe the reported one-electron oxidation process of spiro-MeOTAD$^+$.[21,22,24]

The electronic properties of pristine spiro-MeOTAD films probed by combined techniques of UPS acquired with He−Iα ($h\nu$ = 21.2 eV) source and inverse photoelectron spectroscopy (IPES) are shown in Figure 1. The leading edge of the highest occupied molecular orbital (HOMO) and lowest unoccupied molecular orbital (LUMO) features are at −1.07 eV below and 2.24 eV above the Fermi level (E_F), respectively. Thus, the energy gap between these edges, known as single-particle gap or transport gap,[25] is ∼3.3 eV. From the photoemission cutoff (left-most edge in Figure 1), the work function (ϕ) is found to be 3.9 eV. Finally, the electron affinity (EA) and ionization energy (IE) of the spiro-MeOTAD film are 1.7 and 5.0 eV,[26] respectively. Note that this is the first direct EA measurement by IPES for this material.

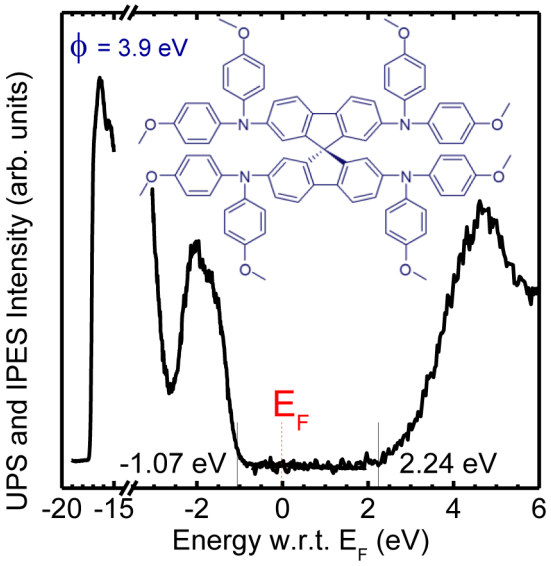

Figure 1. Combined UPS and IPES spectra recorded from a ∼5 nm spiro-MeOTAD film evaporated on SiO_2(native oxide)/Si(100) substrate.

To further investigate the electronic properties, we exposed the pristine spiro-MeOTAD films to various gases. Detailed quantitative analysis, as will be described later, of incorporated oxygen-containing molecules (i.e., O_2 and H_2O) based on the O-1s XPS analysis would be difficult if oxygen-containing substrates (e.g., Si substrates with native oxide) are used. Thus, thermally evaporated Au films (150 nm) on Si(100) were selected as substrates for the spectroscopy studies. The gases, chosen for this project, were ambient air and controlled gas environments such as O_2, N_2, and H_2O (N_2 gas through water bubbler resulting in 100% relative humidity). The gas exposures were done at a pressure of 1 atm and under dark conditions to eliminate photodoping effects.[21,22] The measured relative humidity and temperature of the laboratory where the samples were exposed to ambient air were ∼40% and 22 °C, respectively. Ambient air exposure was conducted through air filters. Once prepared, the gas-exposed films were characterized by UPS and XPS as well as by $I-V$ measurements carried out on field-effect transistors fabricated from these films. First, we discuss the spectroscopy results, followed by the discussion on the transistor results.

UPS measurements were carried out for characterizing the HOMO features as well as the HOMO energy positions with respect to the Fermi level (with regards to E_F) of spiro-MeOTAD(10 nm)/Au for (i) as-grown films and after the different gas exposures of (ii) 25 and (iii) 57 h under dark conditions (Figure 2). The photoemission cutoff and the extended spectra of the valence region can be found in Figure S1 in the Supporting Information. In addition, XPS (Figure 3 and Figures S3−S5 in the Supporting Information) corresponding to the C-1s, O-1s, and N-1s core level was also conducted with the aim to monitor the chemical state of spiro-MeOTAD upon gas exposures. Within the energy resolution of our UPS measurements, similar trends were observed for spiro-MeOTAD deposited on Au and SiO_2 surfaces. The in situ grown ∼10 nm thick spiro-MeOTAD film showed the characteristic HOMO and HOMO-1 orbitals separated by ∼0.5 eV (Figure 2a(i)).[26] Subsequent gas exposure was observed to induce shifts of the Fermi level toward the HOMO features, followed by a gradual decrease in the HOMO intensity. The changes of the electronic properties of the spiro-MeOTAD films induced by the gas-molecule incorporation were monitored by analyzing the binding energy (BE) shifts. Because more than one set of HOMO and HOMO-1 peak fitting parameters lead to the lowest χ^2 results, it was difficult to determine the BE values with sufficient accuracy. In addition, different fitting schemes have been proposed with the presence

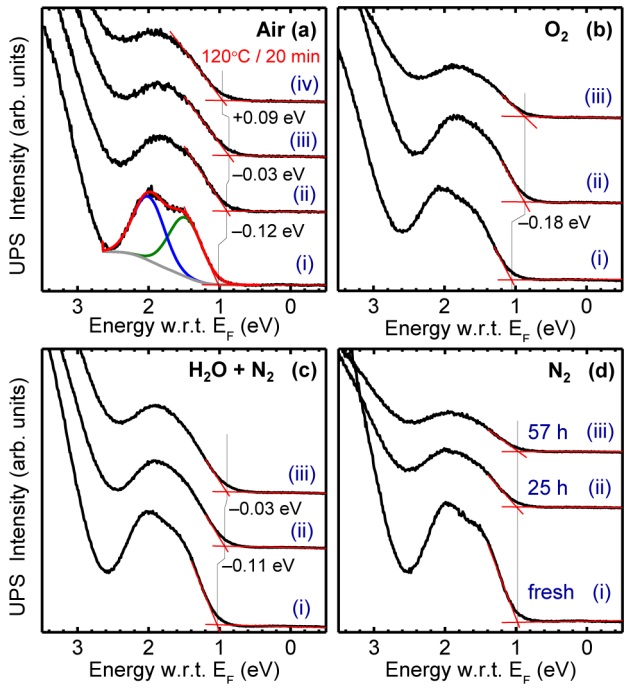

Figure 2. (a) UPS spectra (He−Iα = 21.22 eV) corresponding to the HOMO region of spiro-MeOTAD(10 nm)/Au for (i) the as-grown film and after (a) filtered air and gas exposures of (b) O_2, (c) H_2O + N_2, and (d) N_2 with a total pressure of 1 atm. The time-dependent spectra, (ii) 25 h and (iii) 57 h, shown follow the interaction of the different gases with the spiro-MeOTAD. The relative humidities were ∼40 and 100% during filtered air and H_2O + N_2 exposures, respectively.

dx.doi.org/10.1021/jz500414m | J. Phys. Chem. Lett. 2014, 5, 1374−1379

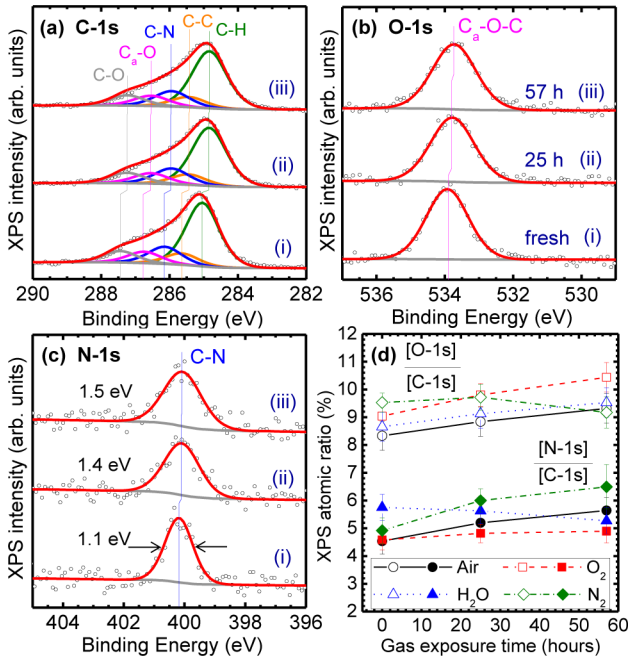

Figure 3. XPS spectra (Mg−Kα = 1253.6 eV) corresponding to the (a) C-1s, (b) O-1s, and (c) N-1s core levels of spiro-MeOTAD(10 nm)/Au at 300 K for (i) as-grown film and subsequent filtered air exposures of (ii) 25 h and (iii) 57 h. (d) XPS atomic ratio variations for O-1s/C-1s[C−N] (open symbols) and N-1s/C-1s (closed symbols) when spiro-MeOTAD is exposed to different gas conditions.

of degenerate states.[27,28] Therefore, we used the HOMO leading edge BE value from each spectrum for comparison purposes. In this way, a total shift of −0.15 eV of the HOMO peak was observed after 57 h of air exposure (Figure 2a). Similarly, exposure to 1 atm of O_2 and H_2O induced shifts in the HOMO peaks toward the Fermi level, as observed in the air-exposed sample, indicating that O_2 and H_2O show some electronic interaction with the pristine spiro-MeOTAD molecules. Spiro-MeOTAD in N_2 did not show changes in the HOMO peak position within the resolution of UPS, indicating weak (if any) electronic interaction between N_2 and the molecule.[29] Although spiro-MeOTAD film shows hydrophobic surface properties determined by water contact angle measurements, we were able to confirm that not only O_2 but also H_2O from the gas phase diffuses into the spiro-MeOTAD film. A summary of ϕ, IE, and HOMO BE changes extracted from UPS spectra are displayed in Figure S2 in the Supporting Information. At first glance, the gradual decrease in the HOMO intensity could be attributed to the change of spiro-MeOTAD chemical structure from the topmost layer (irreversible process). However, XPS and UV−vis measurements did not show any significant changes, confirming that the pristine spiro-MeOTAD structure is chemically maintained under gas exposures. Thus, the changes in the HOMO intensities are associated with the incorporation of gas molecules that attenuate the UPS signal from the underlying spiro-MeOTAD layer. In a separate experiment, the air-exposed sample was heated at 120 °C for 20 min in UHV and remeasured via UPS (Figure 2a(iv)). The HOMO peak was observed to shift backward, and this reversible process was attributed to desorption of surface-adsorbed gas molecules. However, the intensity of the HOMO peak did not recover to its original value, implying the presence of molecules incorporated into the bulk film of spiro-MeOTAD, which is expected to take a much longer time to diffuse out even at elevated temperatures. As a control experiment to rule out the possibility of UV- and X-ray-induced HOMO intensity decrease in pristine spiro-MeOTAD films, an additional spiro-MeOTAD sample was prepared and measured by UPS. The same sample was stored in the UHV chamber for 25 h, and subsequently UPS was remeasured and the intensity was almost the same (i.e., within measurement uncertainty).

Following each UPS measurement, XPS was recorded (Figure 3 and Figures S3−S5 in the Supporting Information). For all freshly prepared spiro-MeOTAD films, all C-1s XPS raw data were fitted considering five components of C−H at 285.1 eV, C−C at 286.2 eV, C−N at 286.7 eV, aromatic C_a−O at 287.3 eV, and C−O at 288 eV. In addition, during the fitting, the intensity ratios of (C−H):(C−C):(C−N):(C_a−O):(C−O) 44:8:12:8:8 (inset in Figure 1) were constrained, and the XPS raw data were well-reproduced by the previously described curve-fitting model, inferring that vacuum thermal evaporation method can lead to similar film quality of the solvent-casting methods.[26] The O-1s core level of the as-grown film shows one component at 533.9 eV assigned to the O atom bound to C atoms in the alkyl group (C−O) and aromatic ring (C_a−O).[26] Finally, the N-1s core levels were fitted considering one component of C−N bound at 400.2 eV. Subsequent 25 and 57 h exposures to filtered air, O_2, and H_2O induced maximum BE shifts of ∼0.2 eV, indicating the presence of surface-adsorbed species as well as incorporation of gas molecules into the spiro-MeOTAD film. The amount of gas molecules incorporated into the spiro-MeOTAD film as well as any eventual chemical changes (e.g., fragmentation or oxidation) induced by the presence of gas molecules were monitored by quantitative analysis based on XPS data. XPS atomic ratios of O-1s/C-1s and N-1s/C-1s (Figure 3d) were calculated based on the peak areas and after proper normalization using atomic sensitivity factors. Each spiro-MeOTAD molecule is composed of 81 C atoms, 8 O atoms, and 4 N atoms (inset in Figure 1a). Thus, the ratio between integrated O-1s/C-1s and N-1s/C-1s areas should result in nominal ratio values of 9.8 and 4.9%, respectively. A trend of increase in O-1s/C-1s and N-1s/C-1s ratios was observed with increasing gas-exposure times, confirming the incorporation of gas molecules. The incorporation of N_2 molecules into the amorphous spiro-MeOTAD films is also corroborated by the observed increase in the full width at half-maximum (FWHM) in the N-1s spectra (Figure 3c and Figure S5 in the Supporting Information) as a function of the filtered air and N_2 gas exposure times. As previously discussed, the incorporation of O_2 and H_2O molecules was observed to induce BE shifts in the core-level peaks as well as HOMO. On the basis of UV−vis measurements, no indication of oxidized spiro-MeOTAD$^+$ species was obtained above the detection limit of the instrument. In comparison, the work by Schölin et al.[27] showed that the addition of 2 mol % of LiTFSI to spiro-MeOTAD spin-coated in air produced high concentrations of oxidized spiro-MeOTAD$^+$ species at the surface with a gradual decrease in concentration deeper into the film. Furthermore, oxidized spiro-MeOTAD$^+$ species were observed to induce the Fermi level shifts as large as −0.8 eV toward the HOMO features. In our studies, a maximum shift of −0.2 eV was observed by UPS and XPS. Thus, the formation of a transient state of spiro-MeOTAD-O_2 complex is suggested.[30,31]

The observed changes in the electronic properties of pristine spiro-MeOTAD induced by the incorporation of gas molecules

dx.doi.org/10.1021/jz500414m | J. Phys. Chem. Lett. 2014, 5, 1374−1379

motivated further investigations of their influences on the charge transport properties. A common strategy to study the charge-transport properties of organic semiconductors is to extract the field-effect mobility from transistor $I-V$ measurements. We aimed at characterizing the gas-induced effects on the hole mobility (μ) values of spiro-MeOTAD films by fabricating two sets of bottom-gate top-contact OFETs. The first set consisted of 50 nm of spiro-MeOTAD evaporated on thermally grown SiO_2 (300 nm). The second set of OFETs consisted of 10 nm of spiro-MeOTAD evaporated on SiO_2 (300 nm), which was subsequently exposed in situ for 120 h either to filtered air or to the controlled environments of O_2, H_2O, and N_2. Following the gas exposure of the initial 10 nm, an additional 40 nm of fresh spiro-MeOTAD was evaporated on top to match the thickness of the first set of OFETs and allow a direct comparison between these two. In both cases, the devices were completed by evaporating 20 nm thick source and drain Au electrodes through a shadow mask. All of the fabricated transistors had a channel length of 100 μm and various channel widths of 3, 5, or 8 mm. A schematic of the second set of devices is displayed in Figure 4a. The rationale behind fabricating the two sets of samples, as previously described, is that in field-effect transistors charge transport occurs in the first few nanometers of the semiconductor closest to the gate insulators interface.[32] Therefore, exposing the initial 10 nm of spiro-MeOTAD to various gases affects those transport layers most strongly, which should manifest itself in the $I-V$ characteristics. All OFET measurements (Figure S7 in the Supporting Information) were performed in air within 1 h after device preparation. To quantify the gas-induced changes in the charge-transport properties of spiro-MeOTAD, we extracted the hole mobility values from the transistor transfer characteristics in the saturation regime (Figure 4b). We exclusively concentrated on the saturation mobility because in the measured linear regime the ratio of the drain to gate leakage current was not high enough for meaningful mobility extraction (Figure S7 in the Supporting Information). The first set of devices (as prepared) showed a $\mu = (4.6 \pm 0.1) \times 10^{-5}$ cm^2/V·s. The mobility values extracted from our OFET devices were lower compared with previous reports. Hole mobility values as high as $\mu = 2 \times 10^{-4}$ cm^2/V·s are reported on spiro-MeOTAD films prepared by solvent deposition techniques.[33,34] Such a difference is most likely due to variations in the fabrication process. For instance, the morphology as well as the concentration of active impurities incorporated in the deposited films varies significantly with the deposition technique. Thus, the mobility values obtained from a solution-processed film may be substantially different from those from a vacuum deposited film. The second set of devices, in which the 10 nm channel region had been exposed to filtered air and controlled environment of O_2 for 120 h, showed a decrease of ~33 and ~24%, respectively, in the mobility values. Furthermore, a drastic decrease of ~63% in the mobility value is observed when spiro-MeOTAD is exposed for 120 h to the extreme conditions of H_2O-saturated (100% relative humidity) N_2. As previously discussed, XPS and UV–visible measurements did not show the changes in the oxidation state of spiro-MeOTAD upon gas exposures. Thus, the OFET results suggest that a mechanism for the diffusion and incorporation of gas molecules is present in the amorphous spiro-MeOTAD films. Those incorporated molecules induce the decrease in the hole mobility most likely due to the creation of trap states.[35] Only a slight decrease in the mobility is observed after the 120 h exposure in N_2. An additional experiment was conducted to probe the diffusion of gas molecules within the spiro-MeOTAD film from the 10 nm exposed layer to the 40 nm layer deposited on top. The air-exposed sample that showed an initial mobility value of $(3.1 \pm 0.1) \times 10^{-5}$ cm^2/V·s was stored in high vacuum chamber (2×10^{-8} mbar). The mobility was remeasured after 48 and 120 h and a systematic increase to $(3.5 \pm 0.2) \times 10^{-5}$ and $(3.7 \pm 0.2) \times 10^{-5}$ cm^2/V·s, respectively, was observed (Figure S8 in the Supporting Information). This increase in mobility is consistent with the out-diffusion of gas molecules from the 10 nm channel region to the 40 nm thick top layer of pristine spiro-MeOTAD.

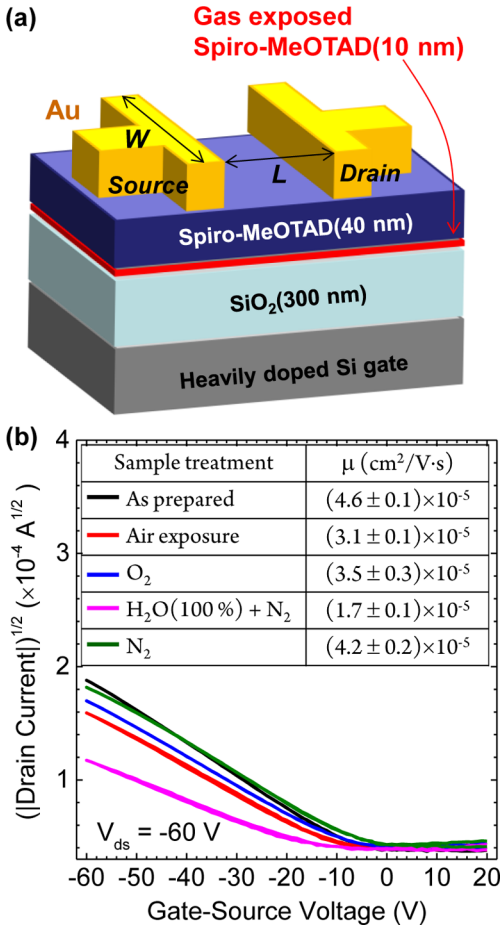

Figure 4. (a) spiro-MeOTAD-based OFET device schematic with a bottom-gate top-contact configuration. The channel width of all devices was L = 100 μm, while three different channel lengths of W = 3, 5, and 8 mm were used. (b) Square root of the absolute value of the drain current $(|I_{ds}|)^{1/2}$ as a function of gate voltage for the W = 3 mm devices. The saturation mobility values were extracted from the slope. Summary of hole mobility values before and after various gas exposures is indicated in the inset.

In summary, the combined techniques of spectroscopy and OFET measurements reveal the incorporation of gas molecules and its strong influence on the electronic structure of the spiro-MeOTAD. The incorporation of O_2 and H_2O induces the Fermi level to shift toward HOMO, similar to p-doping. On the basis of XPS and UV–vis measurements, no indication of oxidized spiro-MeOTAD$^+$ species was observed. Thus, the formation of transient spiro-MeOTAD-O_2 complexes is tentatively proposed. Spiro-MeOTAD-based OFET devices showed deterioration in the hole mobility after gas exposure

dx.doi.org/10.1021/jz500414m | J. Phys. Chem. Lett. 2014, 5, 1374–1379

most likely due to trap states induced by the incorporation of gas molecules. The magnitude of mobility reduction sensitively depends on the species in the gas.

■ ASSOCIATED CONTENT

Supporting Information

Experimental procedures and additional characterization. This material is available free of charge via the Internet at http://pubs.acs.org.

■ AUTHOR INFORMATION

Corresponding Author

*E-mail: yabing.qi@oist.jp.

Notes

The authors declare no competing financial interests.

■ ACKNOWLEDGMENTS

This work was financially supported by Okinawa Institute of Science and Technology Graduate University. Work in Princeton University was supported by a grant of the National Science Foundation (DRM-1005892). We thank DSSC, Advanced Technologies R&D, Merck, Ltd., Japan for proving spiro-MeOTAD for this work.

■ REFERENCES

(1) Cai, N.; Moon, S. J.; Cevey-Ha, L.; Moehl, T.; Humphry-Baker, R.; Wang, P.; Zakeeruddin, S. M.; Gratzel, M. An Organic D-p-A Dye for Record Efficiency Solid-State Sensitized Heterojunction Solar Cells. *Nano Lett.* **2011**, *11*, 1452−1456.

(2) Hsu, C. Y.; Chen, Y. C.; Lin, R. Y. Y.; Ho, K. C.; Lin, J. T. Solid-State Dye-Sensitized Solar Cells Based on Spirofluorene (Spiro-OMeTAD) and Arylamines as Hole Transporting Materials. *Phys. Chem. Chem. Phys.* **2012**, *14*, 14099−14109.

(3) Bach, U.; Lupo, D.; Comte, P.; Moser, J. E.; Weissortel, F.; Salbeck, J.; Spreitzer, H.; Gratzel, M. Solid-State Dye-Sensitized Mesoporous TiO_2 Solar Cells with High Photon-to-Electron Conversion Efficiencies. *Nature* **1998**, *395*, 583−585.

(4) Margulis, G. Y.; Christoforo, M. G.; Lam, D.; Beiley, Z. M.; Bowring, A. R.; Bailie, C. D.; Salleo, A.; McGehee, M. D. Spray Deposition of Silver Nanowire Electrodes for Semitransparent Solid-State Dye-Sensitized Solar Cells. *Adv. Energy Mater.* **2013**, *3*, 1657−1663.

(5) Burschka, J.; Dualeh, A.; Kessler, F.; Baranoff, E.; Cevey-Ha, N. L.; Yi, C. Y.; Nazeeruddin, M. K.; Gratzel, M. Tris(2-(1H-pyrazol-1-yl)pyridine)cobalt(III) as p-Type Dopant for Organic Semiconductors and Its Application in Highly Efficient Solid-State Dye-Sensitized Solar Cells. *J. Am. Chem. Soc.* **2011**, *133*, 18042−18045.

(6) Roelofs, K. E.; Brennan, T. P.; Dominguez, J. C.; Bailie, C. D.; Margulis, G. Y.; Hoke, E. T.; McGehee, M. D.; Bent, S. F. Effect of Al_2O_3 Recombination Barrier Layers Deposited by Atomic Layer Deposition in Solid-State CdS Quantum Dot-Sensitized Solar Cells. *J. Phys. Chem. C* **2013**, *117*, 5584−5592.

(7) Snaith, H. J. Perovskites: The Emergence of a New Era for Low-Cost, High-Efficiency Solar Cells. *J. Phys. Chem. Lett.* **2013**, *4*, 3623−3630.

(8) Park, N. G. Organometal Perovskite Light Absorbers Toward a 20% Efficiency Low-Cost Solid-State Mesoscopic Solar Cell. *J. Phys. Chem. Lett.* **2013**, *4*, 2423−2429.

(9) Kim, H. S.; Lee, J. W.; Yantara, N.; Boix, P. P.; Kulkarni, S. A.; Mhaisalkar, S.; Gratzel, M.; Park, N. G. High Efficiency Solid-State Sensitized Solar Cell-Based on Submicrometer Rutile TiO_2 Nanorod and $CH_3NH_3PbI_3$ Perovskite Sensitizer. *Nano Lett.* **2013**, *13*, 2412−2417.

(10) Liu, D.; Kelly, T. L. Perovskite Solar Cells with a Planar Heterojunction Structure Prepared Using Room-Temperature Solution Processing Techniques. *Nat. Photonics* **2014**, *8*, 133−138.

(11) Liu, M. Z.; Johnston, M. B.; Snaith, H. J. Efficient Planar Heterojunction Perovskite Solar Cells by Vapour Deposition. *Nature* **2013**, *501*, 395−398.

(12) Kumar, M. H.; Yantara, N.; Dharani, S.; Graetzel, M.; Mhaisalkar, S.; Boix, P. P.; Mathews, N. Flexible, Low-Temperature, Solution Processed ZnO-Based Perovskite Solid State Solar Cells. *Chem. Commun.* **2013**, *49*, 11089−11091.

(13) Stranks, S. D.; Eperon, G. E.; Grancini, G.; Menelaou, C.; Alcocer, M. J. P.; Leijtens, T.; Herz, L. M.; Petrozza, A.; Snaith, H. J. Electron-Hole Diffusion Lengths Exceeding 1 Micrometer in an Organometal Trihalide Perovskite Absorber. *Science* **2013**, *342*, 341−344.

(14) Xing, G. C.; Mathews, N.; Sun, S. Y.; Lim, S. S.; Lam, Y. M.; Gratzel, M.; Mhaisalkar, S.; Sum, T. C. Long-Range Balanced Electron- and Hole-Transport Lengths in Organic-Inorganic $CH_3NH_3PbI_3$. *Science* **2013**, *342*, 344−347.

(15) Snaith, H. J.; Moule, A. J.; Klein, C.; Meerholz, K.; Friend, R. H.; Gratzel, M. Efficiency Enhancements in Solid-State Hybrid Solar Cells via Reduced Charge Recombination and Increased Light Capture. *Nano Lett.* **2007**, *7*, 3372−3376.

(16) Yella, A.; Lee, H. W.; Tsao, H. N.; Yi, C. Y.; Chandiran, A. K.; Nazeeruddin, M. K.; Diau, E. W. G.; Yeh, C. Y.; Zakeeruddin, S. M.; Gratzel, M. Porphyrin-Sensitized Solar Cells with Cobalt (II/III)-Based Redox Electrolyte Exceed 12% Efficiency. *Science* **2011**, *334*, 629−634.

(17) Christians, J. A.; Fung, R. C. M.; Kamat, P. V. An Inorganic Hole Conductor for Organo-Lead Halide Perovskite Solar Cells. Improved Hole Conductivity with Copper Iodide. *J. Am. Chem. Soc.* **2014**, *136*, 758−764.

(18) Dewalque, J.; Colson, P.; Thalluri, G. K. V. V; Mathis, F.; Chene, G.; Cloots, R.; Henrist, C. Pore-Filling of Spiro-OMeTAD Determined by Rutherford Backscattering Spectrometry in Templated TiO_2 Photoelectrodes. *Org. Electron.* **2014**, *15*, 9−15.

(19) Ding, I. K.; Tetreault, N.; Brillet, J.; Hardin, B. E.; Smith, E. H.; Rosenthal, S. J.; Sauvage, F.; Gratzel, M.; McGehee, M. D. Pore-Filling of Spiro-OMeTAD in Solid-State Dye Sensitized Solar Cells: Quantification, Mechanism, and Consequences for Device Performance. *Adv. Funct. Mater.* **2009**, *19*, 2431−2436.

(20) Wang, H.; Xu, M.; Liu, G. H.; Li, X.; Xiang, P.; Ku, Z. L.; Rong, Y. G.; Liu, L. F.; Hu, M.; Yang, Y.; et al. Effect of Photo-Doping on Performance for Solid-State Dye-Sensitized Solar Cell Based on 2,2′7,7′-Tetrakis-(N,N-di-p-Methoxyphenylamine)-9,9′-Spirobifluorene and Carbon Counter Electrode. *Electrochim. Acta* **2013**, *99*, 238−241.

(21) Cappel, U. B.; Daeneke, T.; Bach, U. Oxygen-Induced Doping of Spiro-MeOTAD in Solid-State Dye-Sensitized Solar Cells and Its Impact on Device Performance. *Nano Lett.* **2012**, *12*, 4925−4931.

(22) Yang, L.; Xu, B.; Bi, D. Q.; Tian, H. N.; Boschloo, G.; Sun, L. C.; Hagfeldt, A.; Johansson, E. M. J. Initial Light Soaking Treatment Enables Hole Transport Material to Outperform Spiro-OMeTAD in Solid-State Dye-Sensitized Solar Cells. *J. Am. Chem. Soc.* **2013**, *135*, 7378−7385.

(23) Snaith, H. J.; Gratzel, M. Light-Enhanced Charge Mobility in a Molecular Hole Transporter. *Phys. Rev. Lett.* **2007**, *98*, 177402.

(24) Burschka, J.; Kessler, F.; Nazeeruddin, M. K.; Gratzel, M. Co(III) Complexes as p-Dopants in Solid-State Dye-Sensitized Solar Cells. *Chem. Mater.* **2013**, *25*, 2986−2990.

(25) Hwang, J.; Wan, A.; Kahn, A. Energetics of Metal-Organic Interfaces: New Experiments and Assessment of the Field. *Mater. Sci. Eng., R* **2009**, *64*, 1−31.

(26) Hock, R.; Mayer, T.; Jaegermann, W. p-Type Doping of Spiro-MeOTAD with WO_3 and the Spiro-MeOTAD/WO_3 Interface Investigated by Synchrotron-Induced Photoelectron Spectroscopy. *J. Phys. Chem. C* **2012**, *116*, 18146−18154.

(27) Scholin, R.; Karlsson, M. H.; Eriksson, S. K.; Siegbahn, H.; Johansson, E. M. J.; Rensmo, H. Energy Level Shifts in Spiro-OMeTAD Molecular Thin Films When Adding Li-TFSI. *J. Phys. Chem. C* **2012**, *116*, 26300−26305.

(28) Fantacci, S.; De Angelis, F.; Nazeeruddin, M. K.; Gratzel, M. Electronic and Optical Properties of the Spiro-MeOTAD Hole

Conductor in Its Neutral and Oxidized Forms: A DFT/TDDFT Investigation. *J. Phys. Chem. C* **2011**, *115*, 23126−23133.
(29) Bussolotti, F.; Kera, S.; Kudo, K.; Kahn, A.; Ueno, N. Gap states in Pentacene Thin Film Induced by Inert Gas Exposure. *Phys. Rev. Lett.* **2013**, *110*, 267602.
(30) Guerrero, A.; Boix, P. P.; Marchesi, L. F.; Ripolles-Sanchis, T.; Pereira, E. C.; Garcia-Belmonte, G. Oxygen Doping-Induced Photogeneration Loss in P3HT:PCBM Solar Cells. *Sol. Energy Mater. Sol. Cells* **2012**, *100*, 185−191.
(31) Abdou, M. S. A.; Orfino, F. P.; Son, Y.; Holdcroft, S. Interaction of Oxygen with Conjugated Polymers: Charge Transfer Complex Formation with Poly(3-Alkylthiophenes). *J. Am. Chem. Soc.* **1997**, *119*, 4518−4524.
(32) Dhoot, A. S.; Wang, G. M.; Moses, D.; Heeger, A. J. Voltage-Induced Metal-Insulator Transition in Polythiophene Field-Effect Transistors. *Phys. Rev. Lett.* **2006**, *96*, 246403.
(33) Poplavskyy, D.; Nelson, J. Nondispersive Hole Transport in Amorphous Films of Methoxy-Spirofluorene-Arylamine Organic Compound. *J. Appl. Phys.* **2003**, *93*, 341−346.
(34) Snaith, H. J.; Gratzel, M. Enhanced Charge Mobility in a Molecular Hole Transporter via Addition of Redox Inactive Ionic Dopant: Implication to Dye-Sensitized Solar Cells. *Appl. Phys. Lett.* **2006**, *89*, 262114.
(35) Sakanoue, T.; Yahiro, M.; Adachi, C.; Takimiya, K.; Toshimitsu, A. Electrical Characteristics of Single-Component Ambipolar Organic Field-Effect Transistors and Effects of Air Exposure on Them. *J. Appl. Phys.* **2008**, *103*, 094509.